Mai 2015

Influence of surface and crystal structure on the conductivity of individual InAs and InP nanowires

Lena Kral

Department of Physics, Lund University

Bachelor thesis supervised by Dr. Rainer Timm

Co-supervised by Olof Persson and Jovana Colvin

LUND
UNIVERSITY

Abstract

To satisfy the great need for (opto-)electronic devices to become smaller and more efficient in energy and price, research is done on semiconducting III-V nanowires (NWs). Electrical devices using NWs show noteworthy assets being fast-paced with high-speed electronics and low power consumption, one of which are high-efficient solar cells at a moderate price.

Developing electric devices it turns out to be of importance to measure individual NW conductivities for further improvements, if possible even in their upright standing growth geometry. Even though in the past this shaped up to be difficult, a new method was executed: utilizing scanning tunneling microscopy and a top contact method individual NWs are localized and contacted to finally be able to measure their individual conductance behavior.

This new method was employed in this thesis by investigating two NW systems that are promising for application in high-speed electronics and energy harvesting. First the influence of boundary interfaces between wurtzite and zinc blende structures on the conductivity of InAs NWs was investigated. It is shown that these transitions play an important role in combination with the existence of oxides on the surface. Cleaning the NWs with hydrogen results in an unexpected consequence: The current rises significantly with almost two orders of magnitude, going hand in hand with a much larger conductivity. In addition one can observe the current-voltage behavior to become more homogeneous.

Secondly, the influence of a passivation layer coating photovoltaic InP NWs is investigated. Determining an ideality factor of $n = 2,4 \pm 0,2$ confirms the improvement of conductivity caused by the passivation layer. Lastly and contrary to expectations no photovoltaic response of the InP NW sample could be observed which is further discussed.

Acknowledgments

Writing my bachelor thesis was the first contact I had with *real* physical research and to actually having some time to dive deeper into an academical topic. I had the enormous luck of finding myself doing this in a wonderful competent, helpful, sympathetic, and as well interesting as interested team of people which I am deeply grateful for.

To begin with I would like to express my very great appreciation to my supervisor Rainer Timm, who has always had an open door and a great deal of optimism, motivation, and patience to deal with whatever problems occurred (and because this is an experimental work, there were countless unexpected challenges to meet). His support ranged from deluging me with most interesting papers of all kinds, over sitting together in the lab, fixing equipment to skype-calls over the North Atlantic Ocean. Thank you very much!

I also need to offer my special thanks to Olof Persson and Jovana Colvin with whom I have had the great luck to find two amazing (co)-supervisors.
Under Olofs guidance I not only got to know Miraculix (the scanning tunneling microscope I worked with), how to handle, equip and fully bake the system; but I also learned a great deal about the theoretical background of nanowires and their processing. Olof impressed and helped me with his sympathetic combination of a substantiated theoretical knowledge and a very calm hand, being able to mechanically fix the smallest parts (but to locate the edged wires in their holders from time to time). Thank you so much!

Jovana has helped me a lot with her knowledge about InP nanowires, and gave me an idea how it should look like. Encountering intractable Sisyphean tasks, I could always find her in the labs, showing a sweeping delight to mount, build and experimentally work, and finally solve whatever came up. I am very grateful for that.

Like mentioned before, it was also the whole STM group of the synchrotron radiation research and solid state department which shaped the openly productive atmosphere. In this context the weekly and cake-intensive STM meeting always sweetened my day. On a more serious note: I consider it to be especially valuable to work in an environment where one can always ask and brainstorm or get feedback from everyone else. This gives rise to a very creative atmosphere.

None of this research would have been possible without Sebastian Lehmann, Jesper Wallentin, Magnus Borgström, who have grown the samples which I used in this context.

Finally I want to thank Marvin and all my friends for being there, providing energy, support, inspirations and distractions whenever needed.

Contents

Abbreviations

AHC	Atomic Hydrogen Cleaning
CB	Conduction Band
FCC	Face-Centered Cubic Structure
HCP	Hexagonal Close-Packed Structure
LPE	Liquid-Phase Epitaxy
MOVPE	Metal-Organic Vapor Phase Epitaxy
MBE	Molecular Beam Epitaxy
NW	Semiconducting Nanowire
STM	Scanning Tunneling Microscopy
VB	Valence Band
VPE	Vapor Phase Epitaxy
WZ	Wurtzite
ZB	Zinc Blende

Introduction

We are living in times with a great need for devices to become smaller and smaller, with increasing efficiency and lifetime, still being distributed at low prices. As a result nanotechnology has received huge attention[1] promising to revolutionize our daily lives with technological advancements. Providing the capability to manipulate materials on the nanoscale level (in the order of 10^{-9} m) tailors their unique properties.

One important sub field of nanotechnology are semiconducting nanowires (NWs). They are one dimensional rod shaped crystal structures with diameters of several nm and a length up to several μm, see Fig. 1.

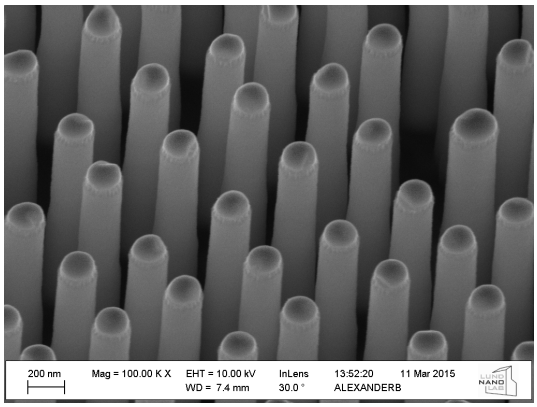

Figure 1: SEM image[(1)]of InP NWs recoded with an angle of 30°. The image size is about $2,8\,\mu\text{m} \times 2,1\,\mu\text{m}$.

In the field of electronics and photonics III-V NWs (consisting of atoms from group III and V in the periodic table) are of special importance.[2–4] Because this field of studies is comparatively young, there is still a lot of fundamental research to be done to tap its full potential.[4] The goal is set on producing ultra-fast diodes and transistors with a low power consumption, as well as LEDs and high-effective solar cells, produced at relatively low prices by consuming only a very small amount of material.

One of the most interesting points about NWs is the fact that these materials can exhibit entirely different material properties as compared to their bulk form, holding great potential for further research and innovative applications. This is mainly caused by their big surface-to-volume-ratio which enhances the influence of surface properties or energy band structures. To properly measure these properties, it is important to evaluate single NWs.

The conductivities of the NWs are measured using scanning tunneling microscopy (STM). But in addition to using it in the conventional way, it is adapted to the special needs, using a recently developed top contact method. In the process the tip is brought in contact with the top part of the wire. By externally applying a bias a current-voltage curve can be recorded. Like this one can monitor the effect of any kind of changes done on the NWs. This stands in contrast to the commonly used method of either finishing the entire cell and then measuring the average conductance over several thousand NWs, or wiping the NWs off their original

[(1)]Made by Jovana Colvin (Division of synchrotron radiation research, Lund university)

substrate, placing them on another one, and finally trying to contact two sides of a single wire, which is difficult to perform in an efficient way.

The aim of the project is to research different influences on the conductivity of III-V NWs. On one side the effect of structural transitions between wurtzite and zinc blende structures in InAs NWs is investigated, as well as the effect of hydrogen-cleaning the NWs in order to remove oxides on the surface. These measurements should be done for at least ten NWs before and after cleaning. The results should then be evaluated, compared to each other and brought into the context of current research.

On the other side the influence of a SiO_2 passivation layer on the conductivity properties of InP NWs is analyzed. The InP NWs are constructed and grown to be implemented in photovoltaic devices with a very similar structure as recently developed solar cells, setting a record for InP NWs.[5] Because of their direct band gap of $1,34\,\mathrm{eV}$ InP is a good material choice for photovoltaic devices, absorbing a large part of the solar spectrum. The aim is to measure at least ten NWs with and without showing a photoelectric response and to compare the results to existing data[6] of a reference sample.

Theoretical background

Looking at different nano-structures, there are a couple of theoretical areas one needs to be aware of before fully understanding the gained results. Considering the two main focuses are nanoscale crystal structures and photovoltaic semiconducting nanowires, some fundamental questions need to be answered: What is a semiconductor? What is a nanowire and what is unique about semiconductor nanowires? How do crystal structures in nanowires look like? And how do photovoltaics play into it? These questions are going to be answered in the following section.[(2)]

2.1 Semiconductors

Different materials can be distinguished by categorizing them in conductors, semiconductors, and insulators. This relates to their ability to conduct electricity. For a further understanding the concept of energy bands is important. In any material, single electrons orbit around the nuclei. The wavefunctions of the individual electrons overlap with the electrons confined to neighboring atoms. Because of the periodic structure of the lattice, a set of closely spaced energy levels is created, forming an energy band. These energy levels are occupied starting with lowest energy band. The highest filled band at $T = 0\,\mathrm{K}$ is called *valence band* (VB). Here the electrons do not participate in the conduction process. The first unfilled band above from the latter is called *conduction band* (CB).

When an electron has enough energy to excite from the valence to the conduction band, it leaves behind a vacancy. This can later be replaced by another electron. The vacancy is called a hole. Both the hole and the electron are considered charge carriers, which move in different directions in an electric field because of their opposite charge.

The valence and conduction band are separated by a band gap. This energy distance determines what category of material one deals with. In an isolator there are as many electrons as there are energy states for them to occupy in the valence band. The energy gap between

[(2)] Further information can be found here.[7]

valence and conduction band is much greater than the thermal energy of the electrons (more than two orders of magnitude). Therefore these materials do not conduct. On the other hand in conductors, like metals, the valence and conduction band overlap, allowing free electrons to participate in the conduction process. Very little energy is required for electrons to occupy new bands. For semiconductors the band gap lays between the one of conductors and isolators.

There are two important groups of semiconductors: Elemental semiconductors, whereas each atom is of the same type (Ge, Si). Here atoms are bound together strongly by covalent bonds and each atom shares one electron with its nearest neighbor. Secondly, there are compound semiconductors made out of two or more elements (GaAs, InP). The compound materials used in this context belong to the group of so called III-V semiconductors, e.g. containing elements found in group III and V of the periodic table. The compound semiconductor bonding is a combination of covalent and ionic bonding.

2.1.1 Doping

The conductivity of a semiconductor can be changed very easily in a controlled manner by the use of doping. In the process impurities are introduced creating a surplus or a deficit of electrons.

An often used example in the industry is silicon, which belongs to the group IV of the periodic table. In the crystal structure neighboring atoms each share a valence electron. If a small amount of an element from group III (acceptor) is added, e.g. B or In, the dopant atom has an insufficient number of bonds to share with Si, like shown in Fig. 2. This causes an excess of free holes. The process of creating positive charge carriers is called *p-doping*. On the other hand one can add an element from group V (donor), e.g. As or P, holding an extra valence electron which it contributes to the crystal. Thereby an excess of free electrons is brought about. This creation of negative charge carriers is termed *n-doping*.

The aim of doping is to shift the Fermi level, which is the hypothetical energy level that has a 50% chance of being occupied by an electron at thermal equilibrium. The method of doping, or more specifically, the energy levels of the dopants, which are located beneath the conduction band (donor) and above the valence band (acceptor), shift the Fermi level. n-doping increases the amount of electrons in the semiconductor, and hence raises the Fermi level. The opposite happens for p-doping. When the differently doped semiconductors are brought in contact with each other the two energy levels converge until the Fermi level is constant in thermodynamic equilibrium. Therefore the valence and conduction band of differently doped semiconductors reveal a bending.

Doping of a compound semiconductor shapes up as a more complicated process. The dopants depend on the site occupied by the atom in the lattice. For a III-V semiconductor atoms of group II act as acceptors when occupying the site of a group III atom; atoms of group VI act as donors while replacing atoms from group V. At the same time dopant atoms from group IV, named amphoteric impurities, can act as acceptors or donors, depending which site they occupy.

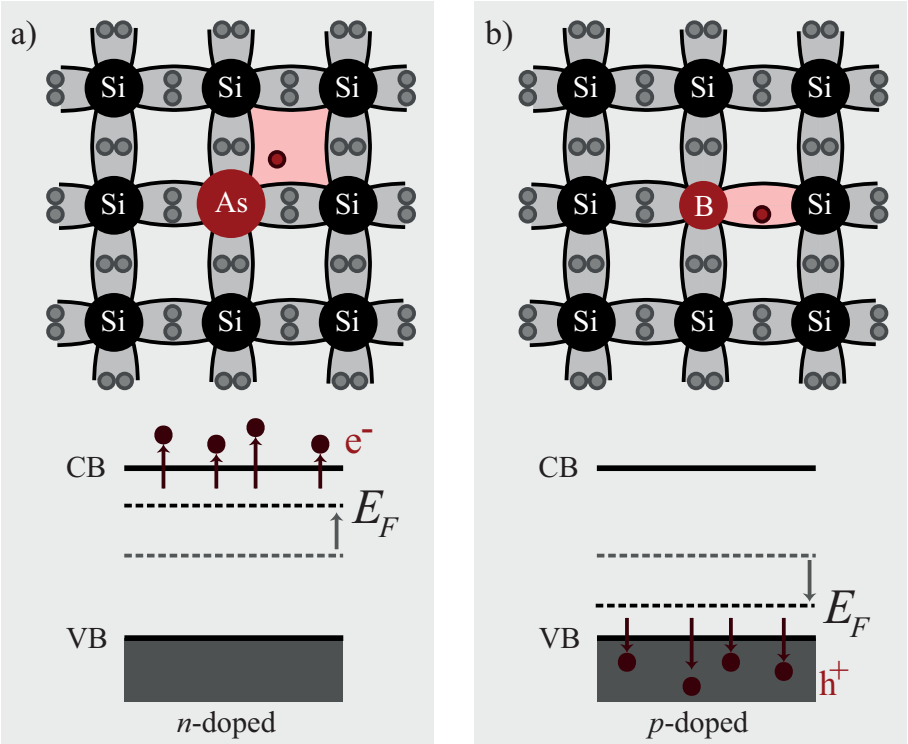

Figure 2: Schematic representation of doping of semiconductors; a) n-doping: using As as a donor to raising the Fermi level, b) p-doping: using B as an acceptor to lower the Fermi level.

2.1.2 Optoelectronic applications

Using the concept of doping, the differently doped parts can now brought in contact with each other. The electrons then start to diffuse from the n to the p-doped part at the junction between them. A depletion region is generated with a local electrical field, making it easier (or harder, depending on the direction) to transport charge carriers through the junction, see Fig. 3. Applying a bias to the p - n junction changes the bending of the energy bands and the size of the depleted region. This knowledge gives rise to a wide variety of applications, like light-emitting diode (LEDs), transistors and photovoltaic solar cells.

LEDs and photovoltaic cells are very much alike in their behavior: In a LED one applies a potential across the p - n junction, causing charge carriers to flow into the depleted region. The electrons recombine with the holes, emitting photons whose energy (and therefore color of the beam light) depend on the band gap size of the material.

The term *photovoltaic* is defined[8] as the "generation of a voltage at the junction of two substances exposed to light" and therefore depicts the converse of a diode. Electron-hole-pairs, with an energy equal to or larger than the band gap, are generated by incoming photons entering the rather broad depletion region. The flow of charge carriers then creates an electrical current. Sunlight consists of a electromagnetic radiation with a wide spectrum of wavelengths. To increase the efficiency of solar cells, several semiconductors with an increasingly smaller band gap (multi-layer structures) are constructed to use the whole spectrum.

2.1.3 I-V characteristics and ideality factor

When looking at diodes or photovoltaic devices one typically looks at their current-voltage (I-V) behavior. The I-V curve of a p-n junction, i.e. a diode, shows a diffusion current I_{diff}

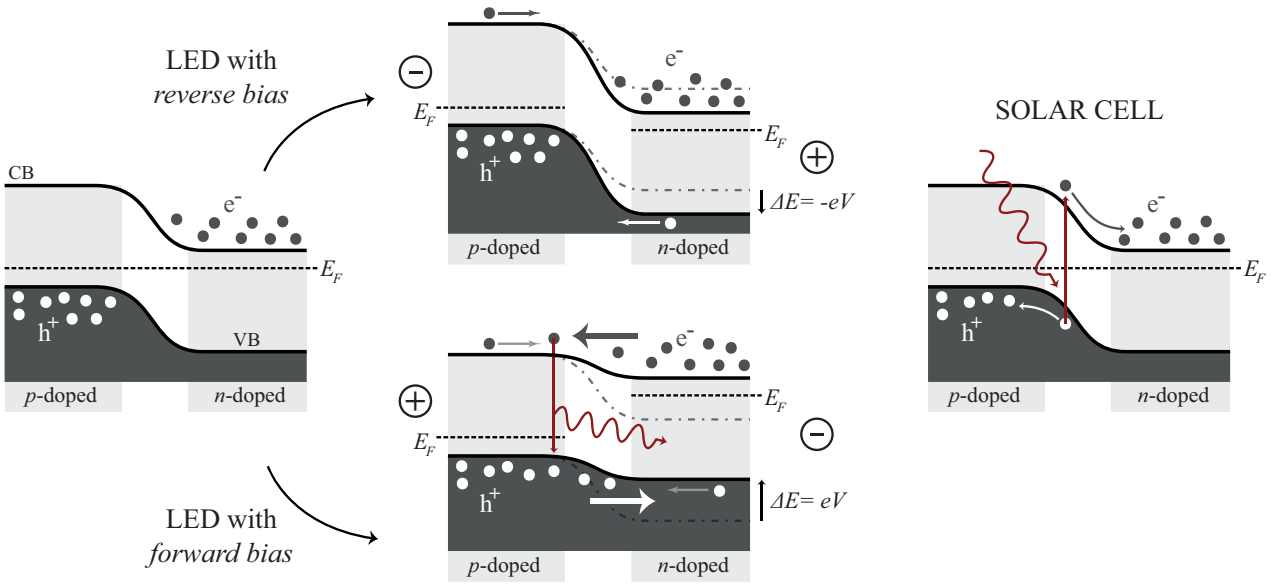

Figure 3: Band diagrams of idealized semiconductor devices, with a p and n-doped region (highlighted) and the depleted region in between. At the left: a unbiased p-n junction, in the middle: a LED with reverse and forward bias, at the right: a solar cell.

and a drift current I_{drift}. When there is no bias applied, both currents equalize; the resulting total current vanishes. Applying a forward bias, the Fermi level of the n-doped part is raised relative to the p-doped part, see Fig. 3. The drift current is not affected by this whereas the diffusion current increases exponentially. Respectively when a reverse bias is applied, the Fermi level of the n-doped part is lowered relatively.

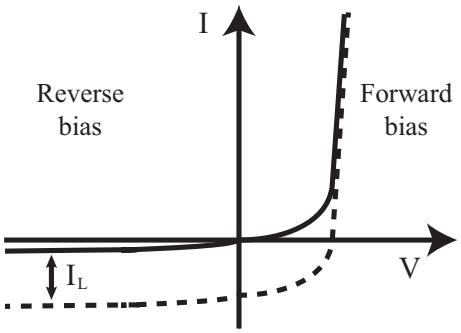

Figure 4: Ideal current-voltage curve of a p-n junction with a current shift, also called a light generated current I_L, in case of a stimulated photovoltaic cell (dashed line) in forward and reverse bias direction.

The theoretical (ideal) diode current behavior $I(V)$, like sketched in Fig. 4, can be described as:

$$I = I_{\text{diff}} - I_{\text{drift}} = I_0 \left[\exp(\frac{qV}{k_B T}) - 1\right] \qquad (2.\ 1)$$

with q being the charge of an electron, k_B the Boltzmann factor, T the temperature, I_0 is the saturation current, and V the applied bias.

Looking at a photovoltaic cell, the photo response of the p-n junction just shifts the I-V curve, mentioned before. So in an ideal case, shown by the dashed line in Fig. 4, an additional light

generated current I_L is subtracted:

$$I = I_{\text{diff}} - I_{\text{drift}} = I_0 \, [\exp(\frac{qV}{k_B T}) - 1] - I_L \tag{2. 2}$$

In reality, several external influences need to be taken into account, e.g. from the metal contact to the p-n junction. For a high voltage in forward direction the Ohmic behavior limits the current. The diode behavior, like described above gets replaced by a linearly increasing curve. The ideal-like diode curve behavior can only be seen when a small voltage is applied.

In order to realize a comparability between different device behaviors, which is going to be very important later in this study, the *ideality factor* n is introduced. n highlights the correspondence between the measured data and the ideal curve. Furthermore I_L cannot be measured directly in reality, as there are losses due to resistance. Therefore one looks at the short-circuit-current $I_{\text{sc}} = I(V = 0)$. Thus in an ideal low resistive solar cell these currents would be equal ($I_L \approx I_{\text{sc}}$). The current can be described as:

$$I = I_{\text{diff}} - I_{\text{drift}} = I_0 \, [\exp(\frac{qV}{nk_B T}) - 1] - I_{\text{sc}} \tag{2. 3}$$

2.2 Nanowires

The Greek word "nano" means dwarf, which seems to be an appropriate word for structures in the scale of about 10^{-9} m, which corresponds to the length of just a few atoms in a solid. Nanowires are structures with two dimensions (the diameter) in the range of $10 - 100$ nm, see Fig. 1. The third dimension, the length of the wire, is much larger and can amount up to several μm. In the following the focus is on semiconducting nanowires (NW). NWs of a particular semiconductor material may behave differently than much larger 'bulk' samples of the same material. They have shown great advantages in effectiveness and cost in many areas, concerning among others the devices mentioned before: LEDs,[9] photovoltaic cells,[10,11] and transistors.[12]

2.2.1 Surface to volume ratio

The surface can play an important role in the properties of a solid. A theoretical infinite, periodic crystal containing only bulk atoms shows well-defined energy states without any disturbances. If the number of surface atoms in reality is small in comparison to the bulk atoms one can still use the theory of an ideal crystal as a good approximation. This however does not hold for nanoscale devices. There one deals with a much bigger surface compared to the bulk portion. Decreasing the size therefore gives rise to new material properties, compared to its material in bulk form, which need to be characterized. Being able to influence the surface structure can result in new, eligible material properties.

2.2.2 Fabrication

There are many ways to produce NWs which can be divided into two main approaches: top-down and bottom-up. In the *top-down* method, NWs are produced via lithography or etching techniques from the bulk material. This was very important in the past decade and it still remains a major factor in the manufacturing of many electrical components. The limitation

of this method is however to be found in the order of 10 nm where it is difficult to create sharp interfaces on an atomic level.

On the other hand there is the *bottom-up* method: within this framework one uses the self-assembling tendency of atoms seeking to become part in bigger structures. It is based on a controlled crystallization process of liquid or solid sources at which nano-structures are being created as particles in the gaseous phase, or on solid surfaces. This method is applied for all NWs mentioned in this thesis.

A common approach for growing free standing NWs in the bottom-up method is to use a particle assisted growth technique in which a metallic seed particle is used to grow the wires.[13] It turned out that gold particles are suited very well for this task, whereas different materials are rather difficult to control.[14]

2.2.3 Epitaxy

To be able to achieve a high crystalline quality of NW, epitaxial growth techniques are often used. Epitaxy is the process of growing single crystals on the surface of a crystalline substrate by maintaining the crystalline structure. This technique is not limited to the growth of NWs but can be also used for bulk devices. The substrate is used to orient the growth of the NWs in an ordered manner. The NWs have the great peculiarity of adopting the same crystalline structure as the substrate it is grown on.[14]

Epitaxy poses a powerful bottom-up method which experienced a strong upswing in the last decade. It facilitates the adjustments of properties like length and diameter of the wires. Various semiconducting materials mentioned before are being used. Most III-V semiconductor NWs are grown this way.[15]

The basic form of epitaxy is the *homoepitaxy*. Here the same material, with different doping concentration, is grown onto itself, being able to form a *p*-*n* junction. On the other hand two (or more) dissimilar materials can be grown on top of each other in the context of *heteroepitaxy*.

There are many methods to use epitaxy. Materials on silicon are usually grown using vapor-phase epitaxy (VPE). For compound semiconductors liquid-phase epitaxy (LPE) is also used. But in the VPE there are more precursors available which moreover can be controlled very precisely. This allows the generation of sharp interfaces between different materials and is therefore the preferred way for III-V NW.[15]

To actually produce NWs there are two alternatives: molecular beam epitaxy (MBE) and metal-organic vapor phase epitaxy (MOVPE). The former technique is generally cheaper and can be performed in a very accurate way. However, its growth speed is much slower[16] which raises the production cost a lot. On this account MOVPE is the preferred method to produce NWs in the industry.[15] Because the wires discussed in this thesis are produced via MOVPE, the procedure is going to be discussed in further detail.

Metal-organic vapor phase epitaxy

Metal organic vapor phase epitaxy involves chemical reactions to promote the epitaxial growth. By varying the gas phase ratio of the precursors one can effectively control the material composition and the doping concentration.[3]

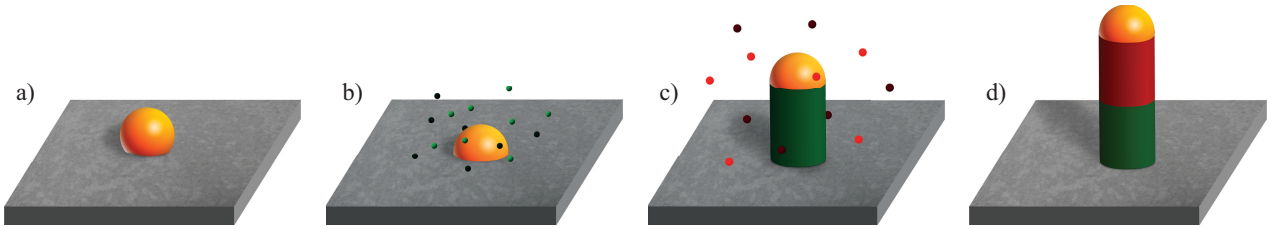

Figure 5: Schematic sketch of a NW growth process using metal organic vapor phase epitaxy.

The process can be seen schematically in Fig. 5 (notice: in reality these NWs have a hexagonal shape). At first the metallic seed particles are deposited on the crystal substrate to locally enhance the NW growth (a).[13] Then the precursors are transported into the system via a carrier gas to the heated substrate (b). The group-III precursors typically consist of metal-organic sources ($Ga(CH_3)$), while group-V precursors can be metal-organic sources or inorganic gases (AsH_3). In the meantime the metallic seed particle has melted and is now on hand in a liquid phase acting as a catalyst. Because of the large accommodation coefficient the gaseous precursors settle preferably under these particles, get absorbed, supersaturate, and finally crystallize (c). By introducing different precursors one can create a more complex axial heterostructure (d).

2.3 Crystal structures

During the epitaxial growth, every solid presents a highly ordered structure, called crystal structure, occurring due to the intrinsic nature of its constituents to form symmetric patterns. It is the materials unique arrangement of atoms, ions or molecules that can strongly influence its properties. Most semiconductors show structural arrangements where the atoms are packed as closely as possible. Closely packed structures are favorable because they secure the highest possible overlap between the valence orbitals of the atoms, maximizing the delocalization of the electrons and thereby the kinetic energy gain. Additionally the number of nearest neighbors for all atoms is maximized, which again gives rise to strongly delocalized states.

The closest possible packing of spheres (as an approximation for atoms) in one dimension is the hexagonal structure, shown in Fig. 6(a). In order to construct a three dimensional structure, a second hexagonal layer is added on top, like shown in Fig. 6(b). For the third layer, there are now two possibilities: the next spheres can be put in the wholes which are on top of the first ones, see Fig. 6(c1), which is then called a hexagonal close-packed structure (hcp). On the other hand it can be put in the other holes next to the first ones, see Fig. 6(c2), which is called face-centered cubic structure (fcc). Both of these two structures have the same packing density and are, in regards to their volume, equally favorable.

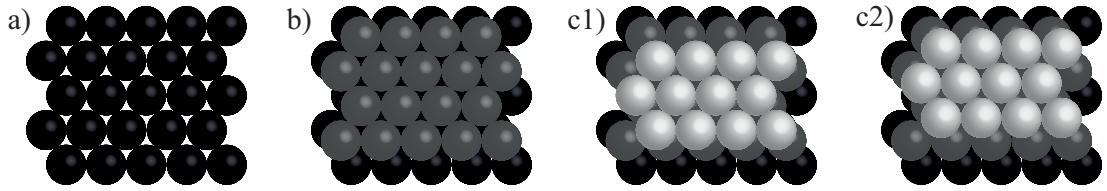

Figure 6: Close packing of spheres in a) hexagonal pattern in one dimension, leading to c1) a hcp structure, or c2) a fcc structure.

Dealing with a material containing different atoms, like the mentioned III-V materials, the

structure usually gets more complex. The two relevant cases are on the one hand when both types of atoms adopt the hcp structure, but are rotated in the so called tetrahedron angle (109.28°) against each other. This structure is called *wurtzite* (WZ). If the same happens with the two types of atoms adapting the fcc structure, which is called a *zinc blende* (ZB) structure.

2.3.1 Nanowire crystal structures

III-V NWs have the peculiarity to show both named structures, being able to crystallize both WZ or ZB, depending on the growth parameters (temperature, doping, gas flux) and diameter.[17] This is contrary to their bulk materials, which appear (because of energetic reasons) generally only as ZB structures. That is the case because NWs grow in the so called 111-direction in which both structures look alike. The other directions are very short and therefore are negligible in finding the ideal energy level, especially in comparison with the surface energies which play a more dominant role at nanometers.

Typically the change between WZ and ZB structures in NWs occurs randomly during the growth, because of the difference in free surface energies of the two structures. It has only recently been found how to control these transitions in a precise way.[18]

Both structures have different electrical properties.[19] To what extent that influences the conductivity of NWs is controversial.[19,20] But because semiconducting NWs are used in many ways in electronics a possible disturbance of the current flow needs to be investigated further.

2.4 Nanowire photovoltaics

In the following will be a short discussion about the applicability of NWs in the photovoltaic industry to underline why NWs are a suitable alternative to bulk material devices.

A very important property in the production of photovoltaic cells (with only few exceptions) is the price/watt ratio. Currently silicon is often used to produce conventional solar cells because it is cheap and the industry is used to machine it. Even though it shows low efficiencies, its price/watt ratio is also relatively low.

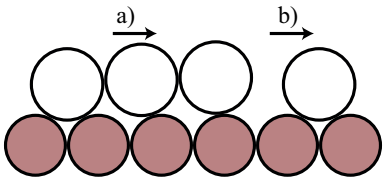

Figure 7: Sketch of the intersection of two materials with different lattice constants.
a) More and more strain is formed, b) until dislocations are created.

There are two problems when working with bulk materials to produce more efficient solar cells (made from III-V compound semiconductors). The material can generally not be grown onto silicon because of their different lattice constants, like shown in Fig. 7. This difference leads to strain between the interfaces causing defects which worsen the performance significantly. The consequence is the usage of highly expensive substrates which cannot be mass-produced in the industry.

A similar problem occurs in the attempt to produce so called 'multi junctions'. Here several materials are placed on top of each other, with increasing band gap size, to use the sun light (consisting of photons with different energies) in a more efficient way. In multi junctions only photons with high enough energies are able to excite electrons in the first material with the greatest band gap. All other photons pass through and eventually excite electrons in the next layers. These different material layers also show deviating lattice constants, causing holes and defects. This can be circumvented with complicated and expensive tricks.

To bypass these problems the use of NWs is a great approach because of their small intersection area with the substrate. The diameter of about $50-100\,\mathrm{nm}$ is small enough to withstand the stress between the atoms, so no dislocations are formed.[21]

Most high end photovoltaic cells in bulk form (using multi-junctions) still show higher efficiencies than photovoltaic devices using NWs; placing a record[22] of over 40%. But their production cost is enormously high.

Because of their potential cost, NW devices are getting more and more important with rising efficiency. As an example the efficiency of GaAs NW solar cells just got doubled within a year from 7,6% in 2014 to 15,3% in 2015.[23,24] The highest efficiency achieved with InP photovoltaic NWs is 13.8% (covering only 12% of the surface).[5]

The initially low efficiency of light absorption and carrier collection[5] has been countered by research in many directions. It was found that the NW diameter and the length of the top n-segment are very important for the performance. Because of the large wavelength of light, the electromagnetic radiation is concentrated in NW, illustrating a high absorption. When placed in an elaborate way, the NWs show an increasing efficiency, lower reflection, and enhanced light trapping.[25,26]

Experimental techniques and procedures

The continuous demand for device performance improvements calls for the development of a wide variety of techniques to observe and measure material surfaces. For the purpose of this project the most appropriate tool is a scanning tunneling microscope. Its composition and practice are treated in this section. Furthermore the specific NW samples are introduced, as well as the experimental techniques which are of importance.

3.1 III-V nanowire samples

The focus of this thesis is on researching electrical properties of single III-V NWs, in as-grown geometry. In this connection the influence of a structural change between WZ and ZB of InAs NWs is being looked at. Also the effect of a passivation layer added on top of photovoltaic InP NWs is researched.

3.1.1 InAs nanowires

The nominally undoped InAs NWs[(3)] are grown on a n-type doped sulfur substrate. The NWs, grown in a similar way like published here,[18] have an average diameter of about $80-100\,\mathrm{nm}$,

[(3)]Made by Sebastian Lehmann (Division of solid state physics, Lund university)

with a length of about 2 μm and are as a majority WZ on the bottom and ZB at the top part like sketched in Fig. 8, and shown in the SEM image in Fig. 9.

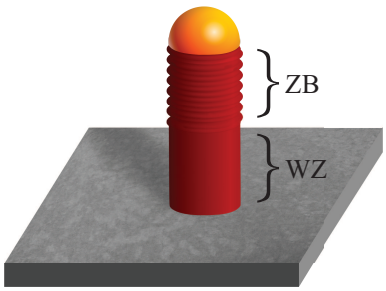

Figure 8: Sketch of a InAs standing NW with a section being WZ, another ZB.

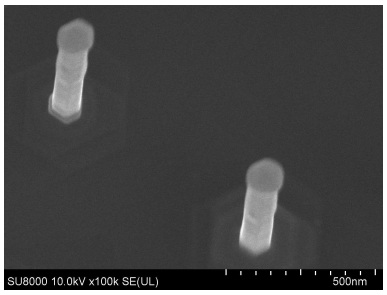

Figure 9: SEM image of standing InAs NWs.[4]

3.1.2 InP nanowires

Secondly a sample of photovoltaic InP NWs is studied. In order to built a solar cell, the removal of the gold particle, as well as adding a passivation layer are part of the production steps. The investigation of these steps therefore acts its part in summon knowledge in order to improve the performance of fabricated solar cells. The InP NWs treated here[5] were grown in the framework of a project, researching the influence of the seed particle (Au) and an added passivation layer (SiO_2) on the conductivity of single InP wires. Hence there are four stages being looked at, like shown in Fig. 10.

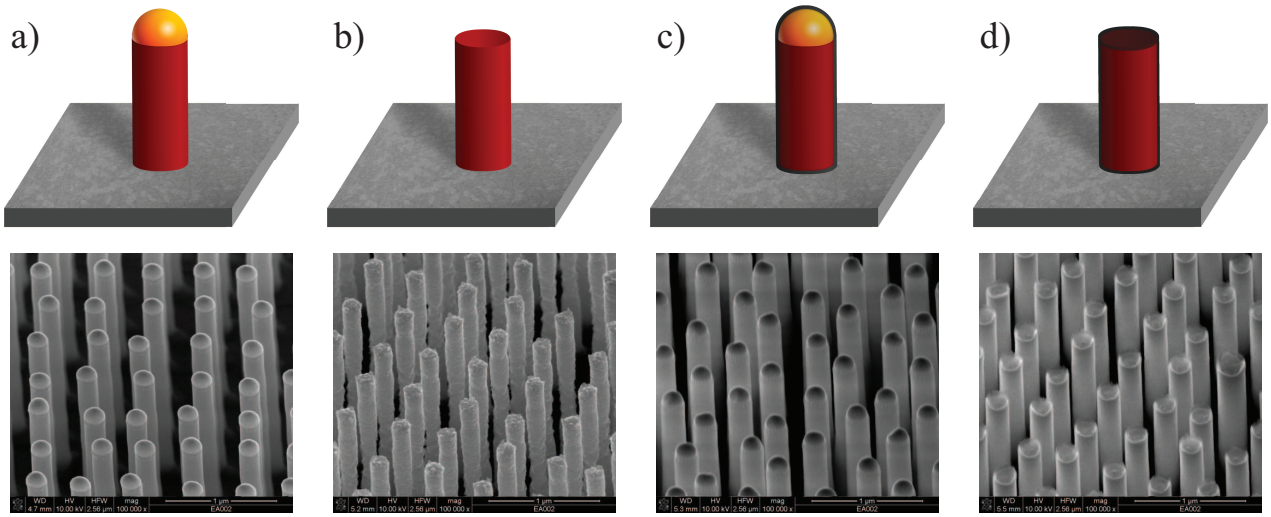

Figure 10: Sketches (above) and SEM images[6](below) of InP NWs a) as-grown, b) after removal of the Au-particle, c) with Au-particle, after SiO_2 layer deposition, d) after Au-particle removal and SiO_2 layer deposition.

[4]Made by Olof Persson (Division of synchrotron radiation research, Lund university)
[5]Produced by Jesper Wallentin (Division of solid state physics, Lund university)
[6]Made by Damir Asoli (Sol voltaics)

The NWs shown here closely resemble those counting to the most efficient NW solar cells ever produced.[5] However the InP NWs studied in this context, are being looked at after growth, but prior to several post-growth processing steps, which further improve the efficiency. Furthermore they have been fabricated using a so called 'selected area growth' to create a regular array of NWs.

Here only the InP NWs with a gold particle and a passivation layer are treated, see Fig. 10(c). InP NWs have a band gap[6] of $1,34\,\mathrm{eV}$, a height of about $1.5\,\mu\mathrm{m}$, and a diameter of 100-200 nm. The InP NWs used for this work were grown epitaxially on Si by the VLS mechanism in Au-assisted selective area metal-organic vapor-phase epitaxy (SA-MOVPE).[6] The nanowires are doped axially, forming a *p-i-n* junction (from bottom to top), having an intrinsic, not doped, part in between. They are separated by about 400 nm.

3.2 Scanning tunneling microscopy

The scanning tunneling microscope was originally invented by Gerd Binning and Heinrich Rohrer in 1982.[27] Four years later they were awarded with the Nobel prize as a valuation for this groundbreaking idea, making it possible to analyze topographic and electronic properties of conducting surfaces with atomic resolution in real space. Scanning tunneling microscopy[(7)] (STM) is based on the quantum tunneling effect where electrons tunnel between a conducting tip and a conducting sample surface.

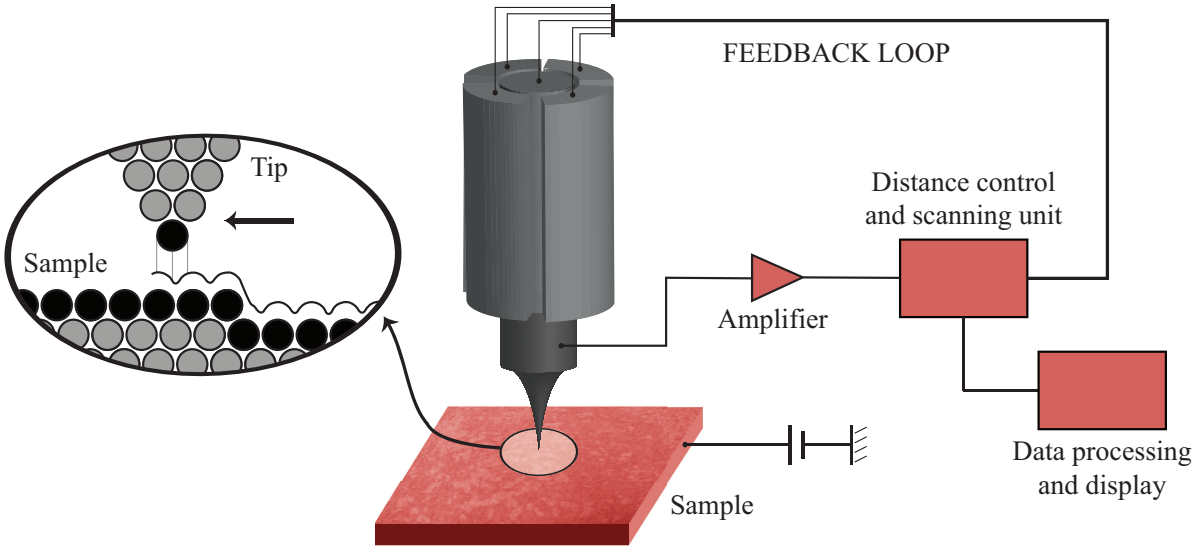

Figure 11: Setting and scanning process of a Scanning Tunneling Microscope.

For a good resolution the tip, usually being made out of tungsten, needs to be atomically sharp, i.e. it has only one atom at the apex like shown ideally on the left side in Fig. 11. To achieve this, a common etching process is used. This is not going to be explained here, but can be gleaned in various papers.[6]

Figure 11 shows the process of STM[(8)], in which the tip is brought close to the surface in a distance of about 10 Å. It can then scan precisely over the surface, accurately driven by

[(7)] For more detailed explanation see.[28]

[(8)] The microscope used in this context is OMICRON UHV STM, controlled by a MATRIX CU V2 controller and the software MATRIX V3.1, respectively

piezoelectric elements which control the height and the x-y scanning movement. In this condition the gap between the tip and sample typifies a barrier for the electrons to tunnel. Now a small tunneling voltage V is applied, causing a tunneling current in the range of pA-nA, depending exponentially on the distance. This current is amplified[(9)] and converted to a high level, low impedance voltage and immediately used as an input to the feedback loop to adjust the tip position. Like this the tip can scan over the surface without crashing into the sample substrate.

To perform successful measurements the whole device must not experience movements or vibrations from the surrounding environment. Therefore a dampening is installed. To do so the scanning tunneling microscope can be hung up on springs. Additionally magnets are used as eddy current brakes in case of a movement to speed up dampening. Usually the measurements take place in a ultra high vacuum chamber to enable clean surface conditions.

3.2.1 Electron Tunneling

The tunneling current I decreases exponentially[29] with tip-sample distance s:

$$I \propto e^{-2s\kappa} \tag{3. 4}$$

where κ is the bias dependent decay rate. Because of this exponential dependence, already a very small difference in distance causes a relatively big and therefore easy detectable current change facilitating a high z-movement resolution. This strongly depends on the tip shape, though.

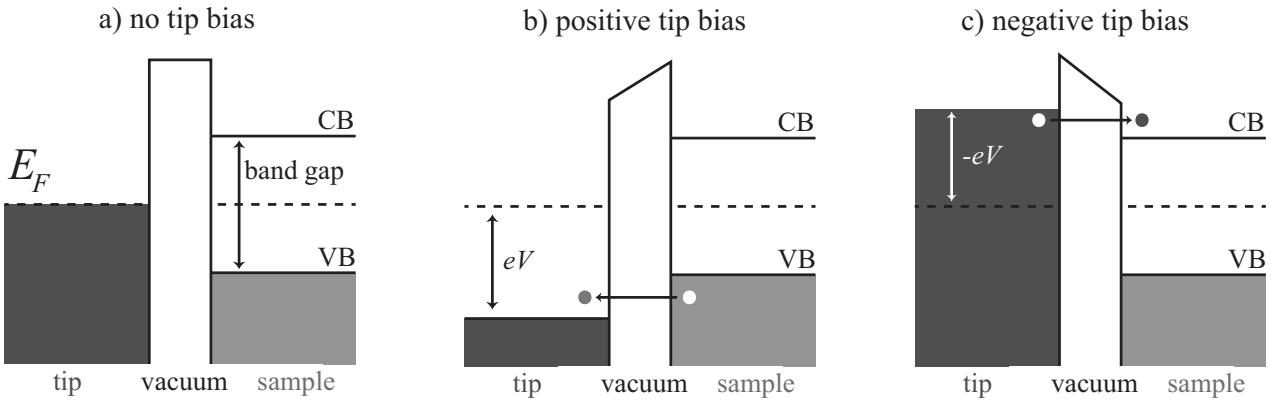

Figure 12: Electron tunneling from filled to empty states for a) no bias, b) positive bias, and c) negative bias applied on the tip.

The direction of current depends on the polarity of the applied bias. When a positive bias (with respect to the substrate) is applied, like shown in Fig. 12(b), electrons tunnel from the filled states of the sample into empty states of the tip, determined by the corresponding densities of states. The same happens vise versa: a negative bias makes the current flow in opposite direction, probing filled electronic states.

3.2.2 Scanning modes

The scanning tunneling microscope records the tunneling current at discrete points while scanning. From the vertical displacement of the tip a topographic image can be constructed.

[(9)] Using the amplifier: SR570

Depending on the topography of the substrate there are different modes/techniques to use.

In this case only the *constant current mode* is of importance and will be discussed. Here the tunneling current is set to a fixed value. By controlling the tip height via the feedback electronics and piezo crystals, the tip will keep the same distance to the substrate to constantly measure this set current value in order to receive the topographic image.

3.3 Top contact method

Characterizing the behavior of nanowires and their properties regarding different surface conditions has been a research goal during the past years. There have been two main approaches: testing conductivity behavior on single wires by wiping them off the growth substrate, placing them on another substrate, and finally attaching small contacts at both ends to do current-voltage measurements.[30,31] The main problem here is the contacts themselves which can diffuse into the wire. It is difficult to know how good the contact actually is, whereas the measurement shows the quality of the contacts rather than the conductivity of the wire. The second attempt has been to go through all processing steps building a finished solar cell, and adding a transparent top contact layer to measure the conductivity. The downside of this method is that there are a million wires measured at the same time. Thus the result is an average and makes it difficult to register small changes applied since all procedure steps need to be finished before the measurement takes place.

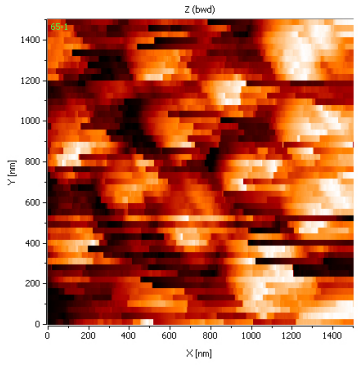

Figure 13: Overview STM image showing the top of InP NWs.

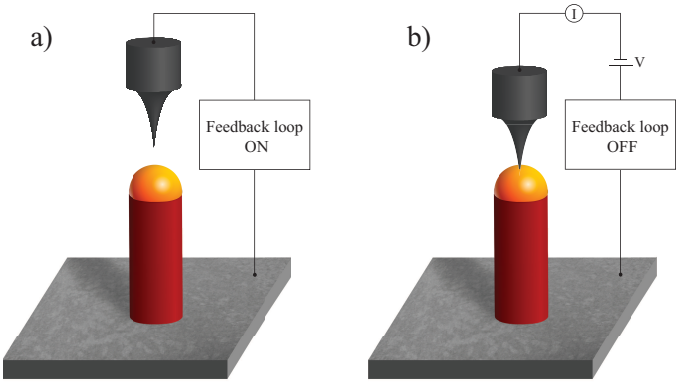

Figure 14: Point contact procedure for standing NWs; a) in constant current mode, b) without the feedback system.

Emanating from these experiences a new approach has been developed[(10)], being sketched in Fig. 14. To start the sample, which is still upright standing on the substrate it was grown on, is approached, choosing the constant current mode. Then the tip is retracted above the expected height, about $1,5\,\mu$m, of the NWs (which requires some experience). This is necessary because the wires are so high that the tip, in case it would scan on the substrate, could not react in an adequate time; resulting for it to crash into the wire.

Having the piezos fully extended, this allows a safe scan over a large area. In an iterative procedure a certain area is scanned, and if no current is detected, the tip approaches (about 200 nm) and so forth. Finally the top of one or several NWs are detected producing an image, like shown in Fig. 13.

[(10)]By Rainer Timm, implemented at this STM by Olof Persson (both: Division of synchrotron radiation research, Lund university)

Getting this far, one NW is chosen for establishing an electrical contact. Now the tip is moved to its center, using the STM reference image for orientation. Furthermore the feedback loop is turned off and the tip is led into the wire. Now the interaction has been changed from a tunneling current to a direct point like contact. An external bias source[(11)], controlled by a Labview program, is used to apply a voltage between the tip and the substrate. The current is then measured while ramping the voltage in order to obtain an I-V curve through the specific wire. The tip is then in controlled steps pushed further into the gold particle on top of the NW to increase the cross section of the tip-sample contact, enabling a greater current flow. Like shown in Fig. 15, the current hereby stabilizes and rises until it finally remains static, showing an Ohmic like contact.[32] Now the preparation to determine the conductivity of the NW is completed and I-V curve(s) can be measured.

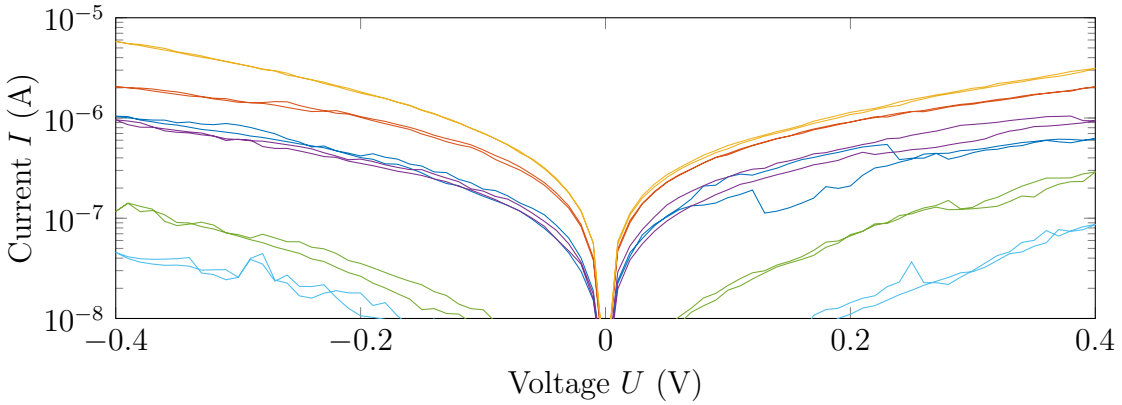

Figure 15: Semilogarithmic I-V curve of an InAs NW showing the progress of first having a very unstable contact (light blue); the tip is then pushed further into the wire until an Ohmic like contact is reached (yellow).

3.4 Illumination

When dealing with photovoltaic cells two I-V curves are recorded: one in the dark, and one with light, i.e. a laser, shone onto it triggering its photovoltaic response, mentioned in section 2.1.3.

To achieve a sufficiently high intensity a mono-chromatic laser diode is pointed at the tip from the outside of the high vacuum chamber onto the boundary point of tip and sample, like shown in Fig. 16(a). This can be done selectively from different angles φ of 20°, and 30°. To further increase the angle a reflective piece of Si is positioned on the ground in front of the STM. The laser then points at the silicon using the reflection to illuminate the sample, like shown in Fig. 16(b).

The angle dependence has been shown[33] to be a critical point in the process. The arriving light needs to enter the depleted region, not only the tip of the NW. Therefore one needs to make sure that no shadowing (neither of the other NWs, nor the tip) takes place.

A shift of the I-V curve is expected as the NWs begin to generate power. After the data is recorded (with and without illumination), the tip is retracted, the feedback loop is turned back on, and the focus is on finding the next wire.

[(11)] SR830 DSP Lock-In Amplifier

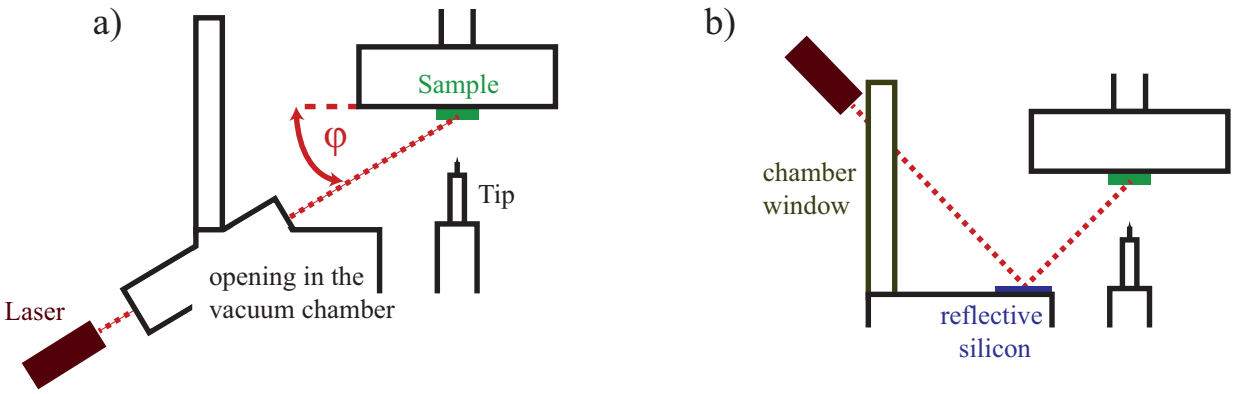

Figure 16: Setup to illuminate the sample a) through an opening pointed at the sample, b) with the help of a reflecting Si piece.

3.5 Surface cleaning

When exposed to air, most III-V semiconductor materials are oxidizing, forming a native oxide of 1-2 nm thickness at the surface.[16] It has been shown how the performance of *p-i-n* junctions of InP NWs is greatly improved upon removal of the surface oxides.[32] Therefore it is of high importance to clean the NWs when studying their facets; or on the other side it is important to investigate how surface states on the NWs affect the devices performance, like done in this thesis.

There are different techniques to clean a crystal surface. One technique, which has often been used for metal crystals, is Ar-ion sputtering.[34,35] This however is inept for III-V semiconductors, because it induces amorphous layers as well as defects which are hard to heal by annealing.[34]

The most eligible process[36] turned out to be atomic hydrogen cleaning (AHC) done inside the high vacuum chamber[(12)]. Here the sample is annealed (for both InP and InAs for 20 min to $\approx 650\,\mathrm{K}$ at $5 \cdot 10^{-6}$ bar) under a flux of atomic hydrogen radicals (H^*) with the help of a thermal cracker (at ≈ 2000 K). The H^* react with the surface oxides leaving behind a clean surface. Because the H^* have low kinetic energies (less than 1 eV), they interact only with the top surface layers.

Here this technique has been used for researching InAs NWs but not in connection with InP NWs. That is because these specific InP NWs already have a passivation layer on top, preserving them from oxidation.

3.6 Interpretation of *I-V* curves

I-V characteristic curves are generally used as a tool to determine and understand the basic parameters of a device also by comparing them to mathematical models. There are two important response curves to mention in this context: the characteristics of a resistor and a diode.

[(12)] Done with the hydrogen atom beam source: HABS-A5-2119123 by Dr. Ebel MBE -Komponenten GmbH

3.6.1 Characteristic of a resistor

A homogeneous resistor, or in this case an un-doped InAs NW, shows theoretically a constant resistance and hence a constant slope in the I-V curve, like shown in Fig. 17. Figure 18 shows the absolute value of the same curve in semilogarithmic scale. The latter is useful looking at characteristics when working with data in different orders of magnitude, whereas the linear plot helps to spot Ohmic-like behavior.

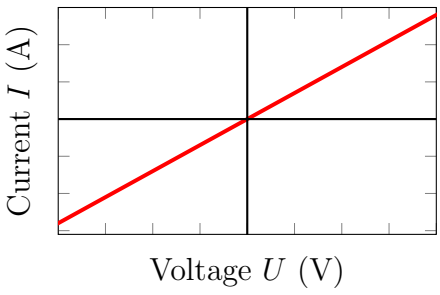

Figure 17: Ideal I-V behavior of a resistor in linear scale.

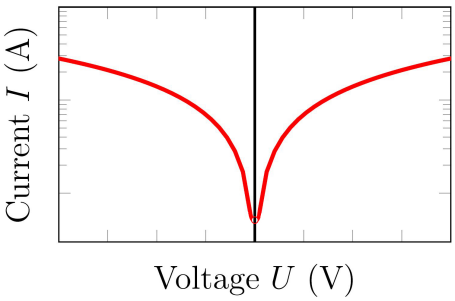

Figure 18: Ideal I-V behavior of a resistor in semilogarithmic scale.

3.6.2 Characteristic of a diode

Diodes, or here doped p-n junctions of InP NWs, show a theoretical behavior like explained in Eq. 2. 1 and shown in Fig. 4. Hence one receives linear and semilogarithmic plots, like shown in Fig. 19, and Fig. 20. Again both plots have their advantages in pointing out different characteristics.

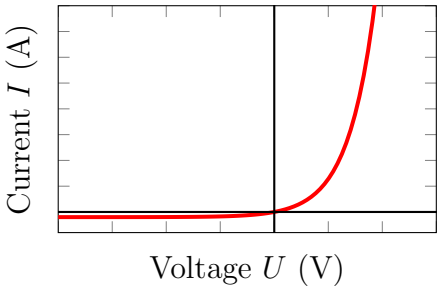

Figure 19: Ideal I-V behavior of a diode in linear scale.

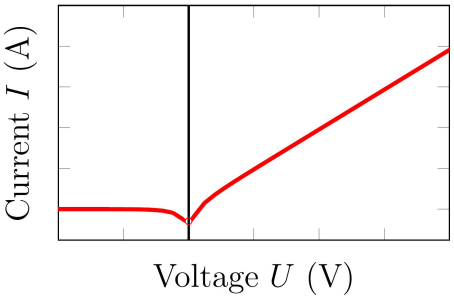

Figure 20: Ideal I-V behavior of a diode in semilogarithmic scale.

Results and discussions

In the following section the discussed theory and all explanations about methods, equipment, and interpretation of data come down to the application. The gained results are going to be shown, analyzed, and discussed. In this work, the I-V characteristics for both, InP and InAs NWs were measured via the top contact method, described in section 3.3.

4.1 Conductivity behavior of InAs NWs before and after cleaning

When looking at InAs NWs with a uniform structure, it has been shown[32] that an Ohmic contact can be reached, using the top-contact method. The question sought to be answered, regards the influence of WZ and ZB structures both being implemented in InAs NWs. Do their boundary surfaces have a disruptive effect on the conductivity of the NWs?

4.1.1 Oxidized InAs nanowires

In order to investigate the interplay of crystal phase and surface structures at first a sample of oxidized InAs NWs with one ZB and WZ segment, as described in section 3.1.1, was looked at. With the mentioned methods the I-V curves shown in Fig. 21 and Fig. 22 were recorded. The data was measured applying a positive bias U_t with respect to the ground on the tip. For a better comparability the same NWs are each depicted with the same colors in both figures.

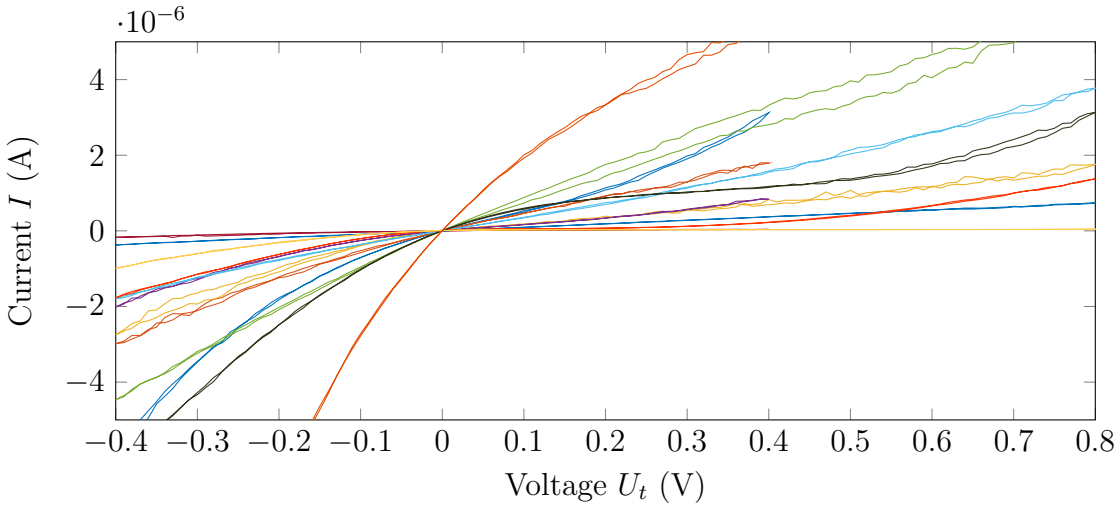

Figure 21: Linear I-V curves of single oxidized InAs NWs before cleaning, with every line referring to a different NW.

Comparing the recorded data with the theoretical graphs of the resistor shown in section 3.6, one can clearly see most curves resemble the theory and show an Ohmic-like characteristic. On the other side there are four exceptions, that is one third of the measurements, showing very non-Ohmic behavior, i.e. at least one inflection point in the semilogarithmic plot. One explanation for this behavior are the NWs themselves: even though the aim was to have a single transition between WZ and ZB towards the middle of the NWs, there are some wires showing no or several transitions due to problems during the growth. This is one idea to explain this unexpected behavior.

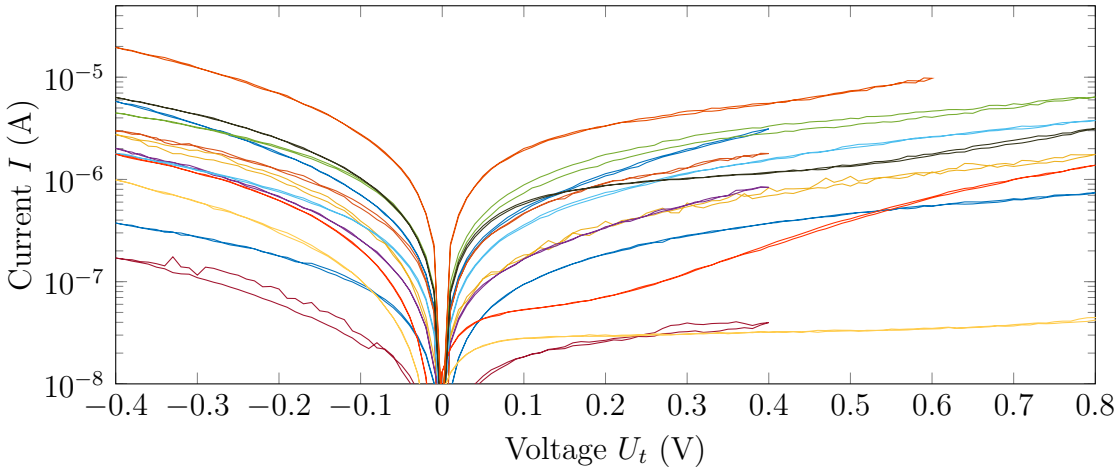

Figure 22: Semilogarithmic I-V curves of single oxidized InAs NWs before cleaning, with every line referring to a different NW.

To further analyze the data and for a better overview the different curves are separated by these two characteristics, shown in Fig. 23 and Fig. 24.

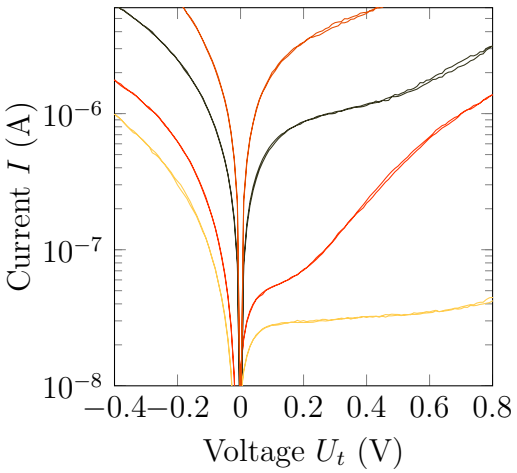

Figure 23: Four oxidized InAs NWs showing non-Ohmic behavior.

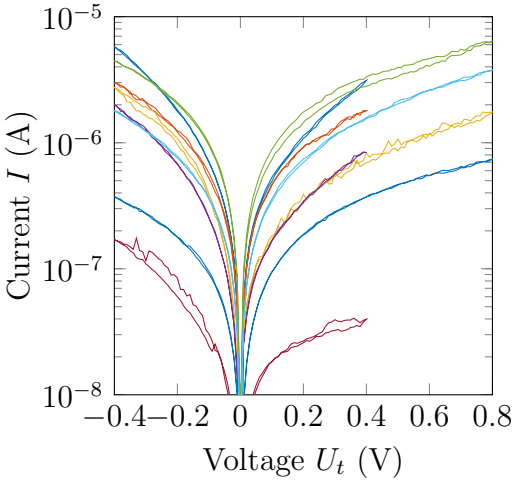

Figure 24: Eight oxidized InAs NWs showing Ohmic like behavior.

It has been shown that InAs NWs conduct mostly over their surface states. To investigate if the transitions between WZ and ZB structures have a disruptive effect on the conductivity, a closer look must be given mainly towards the surface of the NW at the interface line between the two structures. ZB and WZ have slightly different band gap sizes. If the NW is oxidized, which is the case here, the conduction band edges are pinned, being called 'Fermi level pinning'. Hence they cannot flatten when brought in contact with each other.

To quantify the observed I-V behavior, the resistances of the single wires R_n in Fig. 24 can be determined using a linear fit to each curve.

The following values were gained (using Matlab and the least square fit method):

$$R_1 = (109 \pm 6)\,\mathrm{k\Omega} \qquad R_2 = (176 \pm 6)\,\mathrm{k\Omega}$$
$$R_3 = (338 \pm 37)\,\mathrm{k\Omega} \qquad R_4 = (328 \pm 20)\,\mathrm{k\Omega}$$
$$R_5 = (119 \pm 4)\,\mathrm{k\Omega} \qquad R_6 = (231 \pm 6)\,\mathrm{k\Omega}$$
$$R_7 = (3884 \pm 337)\,\mathrm{k\Omega} \qquad R_8 = (1092 \pm 7)\,\mathrm{k\Omega}$$

There are two NWs showing a very high resistance R_7 and R_8. This could be caused by systematical errors, because the tip was not centered accurately and therefore touched the NW with a much larger contact area at its side, or the NW simply bent itself while the STM tip was pushing it down, falsifying the result. On the other side there could also have been an issue with the NW itself consisting of a bad growth structure, showing defects and dislocations and therefore being insignificant to the analysis. With the exception of these two resistances, a mean value of 217 kΩ is recorded.

4.1.2 Cleaned InAs nanowires

In a second step the wires were cleaned with atomic hydrogen, like described in section 3.5. The gained data is shown linearly in Fig. 25, and in a semilogarithmic scale in Fig. 26. Again the same colors in these two figures correspond to the same NWs, which are not the same ones like measured before the cleaning, though.

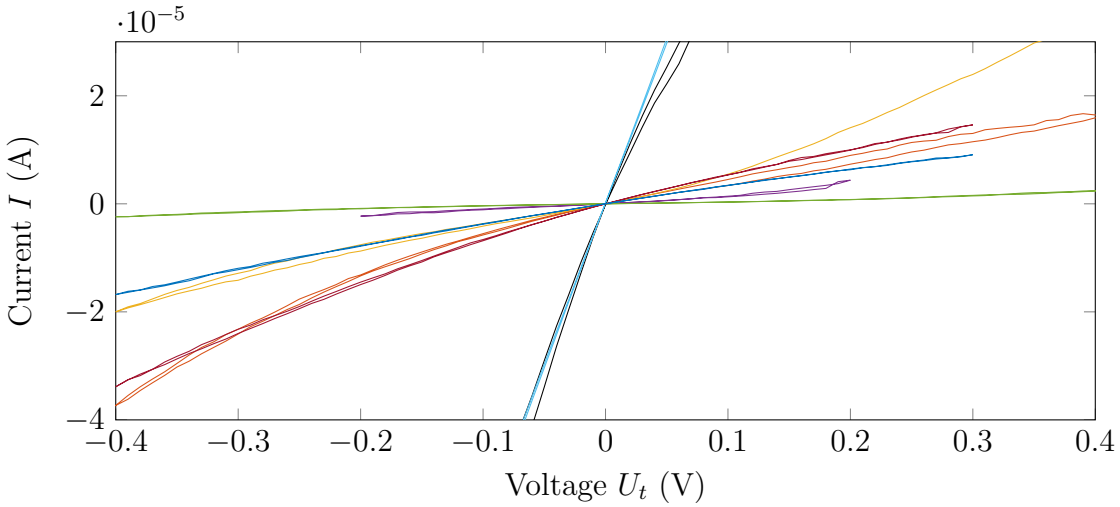

Figure 25: Linear I-V curves of single InAs NWs after cleaning.

Now two things can be observed: First of all, for all measured curves the rectifying behavior seen before is gone, leaving all wires with an Ohmic like behavior.[(13)] To explain this one should be aware of a paper,[19] which researches interfaces of WZ and ZB in InAs NWs finding no measurable energy band edge between the two structures. We therefore postulate in the process of hydrogen cleaning InAs NWs, the conduction bands to shift to flat band conditions, which was not possible before because of the Fermi level pinning of the energy states.

Secondly, one could expect the conductive oxides, such as In_2O_3, to increase the conductivity of the NWs. But the contrary is the case; the current rises significantly upon cleaning showing

[(13)] The fact of I-V curves becoming more homogeneous has also been observed in current research by Olof Persson.

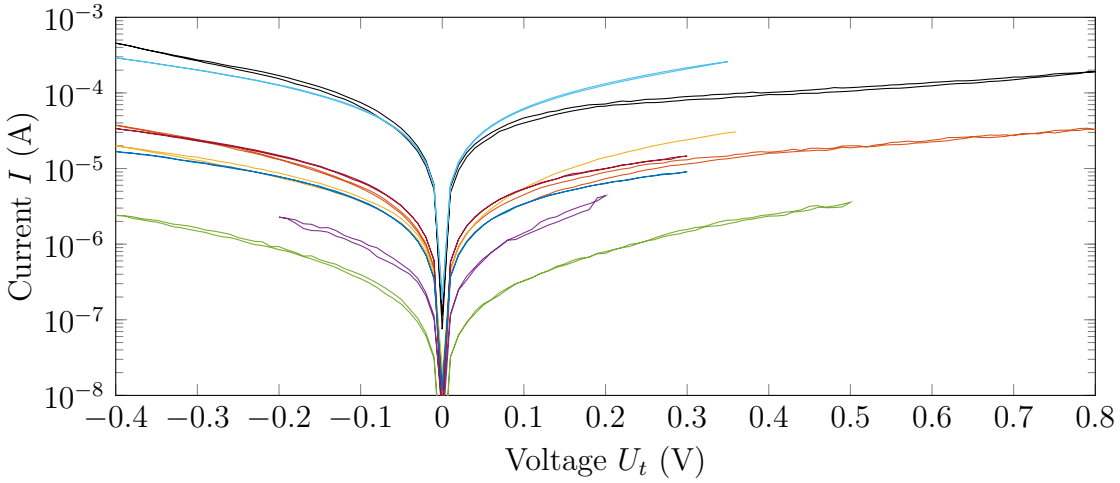

Figure 26: Semilogarithmic I-V curves of single InAs NWs after cleaning.

much lower resistances, which are tabulate below:

$$\begin{aligned} R_1 &= (2,5 \pm 0,4)\,\mathrm{k\Omega} & R_2 &= (20 \pm 1)\,\mathrm{k\Omega} \\ R_3 &= (17,1 \pm 0,6)\,\mathrm{k\Omega} & R_4 &= (72 \pm 1)\,\mathrm{k\Omega} \\ R_5 &= (180 \pm 7)\,\mathrm{k\Omega} & R_6 &= (1,51 \pm 0,02)\,\mathrm{k\Omega} \\ R_7 &= (14,7 \pm 0,4)\,\mathrm{k\Omega} & R_8 &= (26,9 \pm 0,5)\,\mathrm{k\Omega} \end{aligned}$$

Again there are two resistance values R_4 and R_5 which are significantly higher than the others. Suspending those, a mean value of 13 kΩ yields. As a comparison: it was shown[32] that undoped InAs NWs (irrespective of their growth structure) showed a mean resistance of 430 kΩ. This emphasizes the great potential of InAs NWs when considering their initial growth structure.

There is still a noteworthy differences within the measurements on the NWs before and after cleaning. This is caused by the differences in the growth process whereas distinctions in diameter[5] as well as structural differences are critical for the device performance.

The resistances before cleaning are about 20 times greater in their mean value than the resistances afterwards. This can also be seen in Fig. 27, where the recorded data is plotted together with the mean values, calculated from all recorded Ohmic-like behaving data.

There are several reasons for this increased conductivity after cleaning the NWs. The resistances measured here correspond well to the results found[31] in 2010 regarding the order of magnitude of the resistance of single InAs NWs in an oxidized state. Also the effect of a decrease in resistance when the sample oxides were reduced was recorded. Additionally, a similar effect like it was monitored here has been shown:[37] It was found that mixtures of WZ and ZB 'can exhibit up to 2 orders of magnitude higher resistivity than single-phase nanowires' both being looked at in an oxidized condition. During the cleaning process here, the oxides are removed, liberating the NWs from the Fermi level pinning[38] on their surface. Now that the energetic barrier is purged, the conductivity increases strongly. Because we also found a high change in resistivity one can assume the cleaning process to relativize the conductance barrier caused by the interaction with the oxides provoking the NWs to act more like single-phased NWs.

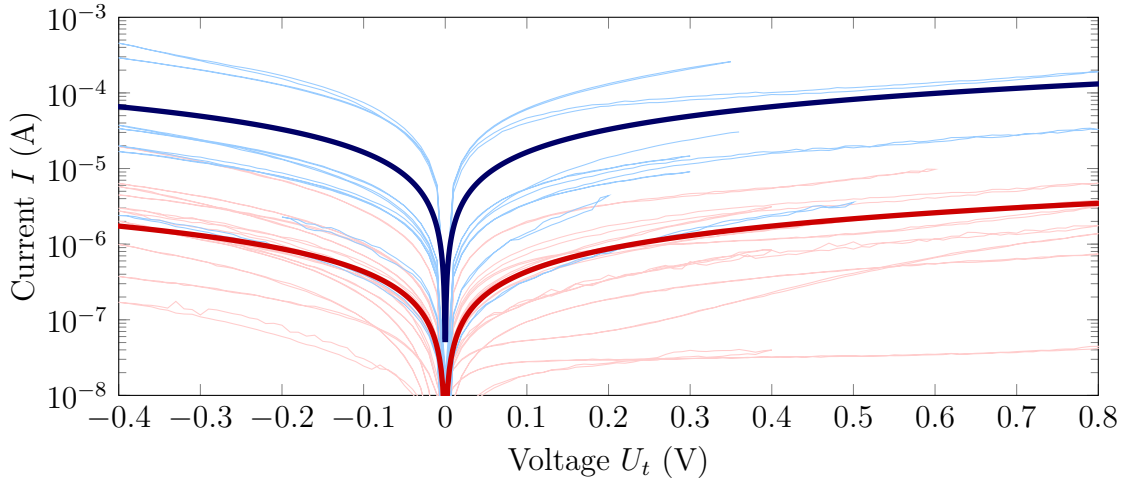

Figure 27: Quantitative comparison between I-V measurements before (red) and after (blue) cleaning with mean values highlighted.

4.2 Conductivity behavior of InP nanowires

Looking at doped InP NWs with p-n junctions, a typical diode like behavior can be seen. Because the InP NWs, described in section 3.1.2, are constructed for implementation in photovoltaic applications, the ideality factor, stating how close the InP NWs follow an ideal diode behavior, is investigated as well as the photo-response behavior of the NWs.

4.2.1 Ideality factor of InP nanowires

For an overarching understanding of the gained data, the I-V curves of various investigated NWs are plotted both linearly in Fig. 28, and semilogarithmic in Fig. 29, at which the same colors correspond to the same NWs in both plots.

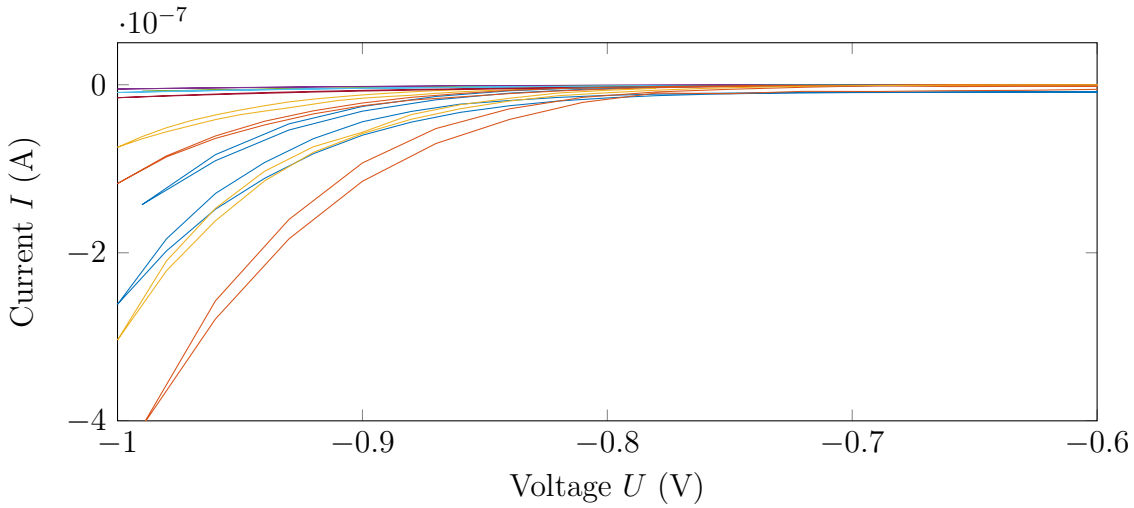

Figure 28: Linear I-V curves of single InP NWs.

Figure 28 shows nice, diode-like curve behaviors. Looking at Fig. 29 this assumption is being confirmed by the straight looking slopes for voltages smaller than $0,6\,\mathrm{V}$, or $0,8\,\mathrm{V}$ respectively, and the negligible small current at positive (reverse) bias. At this point it needs to be added

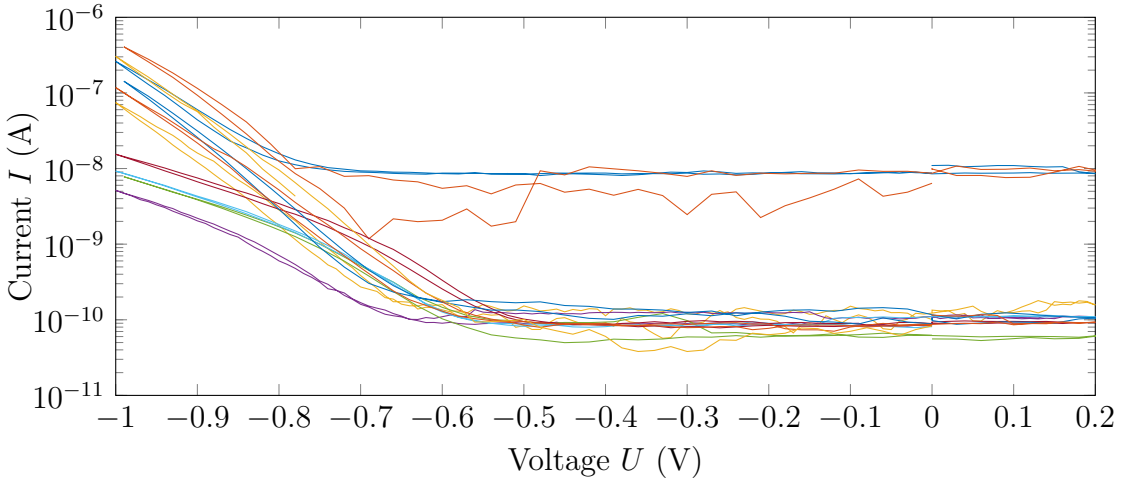

Figure 29: Semilogarithmic I-V curves of single InP NWs.

that because of the positive bias, applied to the tip, the reverse and forward bias appear reversely than sketched in Fig. 4. At first sight one spots two curves having a current of about 10 nA at 0 V, whereas all other wires show a current of roughly $0,1$ nA. This is most likely caused by setting a wrong amplification value, which is done manually for every measurement. For the following plots and calculations they are shifted to the same ground level, like the other curves. Because of significant noise in the order of 10^{-10} A their curves are going to be displayed only for the larger current region (-1 V to $-0,6$ V).

Furthermore the current level at -1 V distinguishes the obtained curves into two groups with similar magnitude, like emphasized in Fig. 30, where the high current red curves are going to be referred to as *group I* and the lower current blue curves will be named *group II*. All I-V curves from group I show a relatively constant slope, whereas the I-V curves in group II show a bending between two linear parts, like shown in Fig. 31. Analyzing the curves in Fig. 29 there is on one side this big division between group I and group II and on the other side a variation in current within these two groups.

The former division is based on a behavior described in section 2.1.3: The current in forward direction is limited by the Ohmic behavior of the diode. The exponential increase gets replaced by a linearly increasing curve. Therefore the current regime in group II with the shallower slope (red part in Fig. 31) is based on losses coming from a high series resistance.

The differences in current within the two groups, e.g. at -1 V can be explained by growth differences between the wires, but also with how the tip was approaching this sample. The InP NWs are standing very close to each other on the substrate, see Fig. 10. Whenever the STM tip has approached, arriving between two NWs it still interacts with both wires at the sides, preventing it to approach further. (Hence the STM tip does not ever reach the substrate.) The recorded STM images only show the top part of the wires in a depth of about $20 - 50$ nm. Therefore it is very difficult to aim exactly for the center of a wire. Especially with a blunt tip it can happen to touch several wires while measuring. Thus the current values also differ as well within the two groups.

In order to evaluate the ideality factor n of the NW diodes, it is included in Eq. 2. 1.
One obtains the straight-line equation:

$$\ln I = \ln I_0 + \frac{q}{nk_BT} V \tag{4. 5}$$

From the slope estimation, mentioned before, one can calculate the ideality factor. The closer

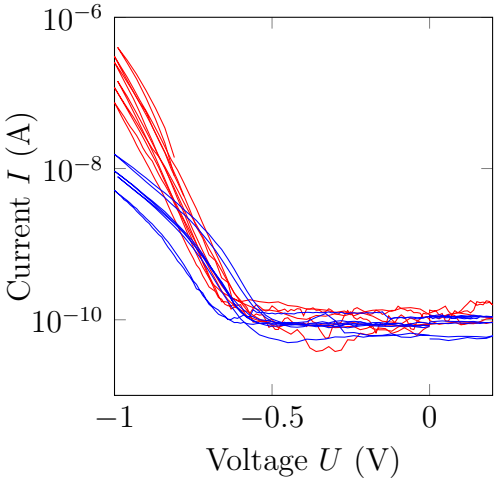

Figure 30: I-V curves divided in group I: higher current (red) and group II: lower current (blue).

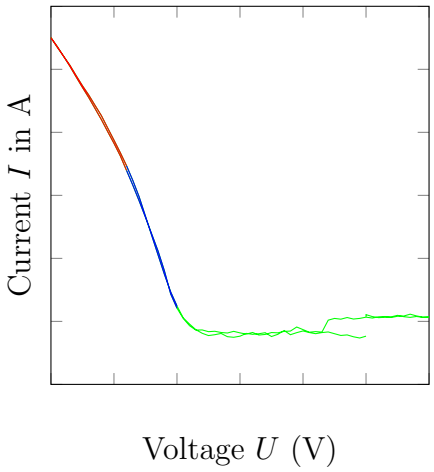

Figure 31: Two slope areas of group II I-V curves: blue part (marked with *) and red part (marked with an a).

the ideality factor is to 1, i.e. the steeper the slope, the more 'ideal' is the measured curve in relation to the theoretical one. For all group II I-V curves, two separate factors are calculated:

$$\underbrace{\begin{aligned} n_1 &= 2,4 \\ n_2 &= 2,2 \\ n_3 &= 2,1 \\ n_8 &= 1,9 \\ n_9 &= 2,3 \\ n_{10} &= 2,1 \end{aligned}}_{\text{group I}} \qquad \underbrace{\begin{aligned} n_4^* &= 2,8 & n_{4\text{a}} &= 4,2 \\ n_5^* &= 2,9 & n_{5\text{a}} &= 4,4 \\ n_6^* &= 2,7 & n_{6\text{a}} &= 4,6 \\ n_7^* &= 2,6 & n_{7\text{a}} &= 4,8 \end{aligned}}_{\text{group II}}$$

Only taking the ideality factor values of the versions of exponential increase (marked with *) for group II, a mean value of $n_{\text{tot}} = 2,4 \pm 0,2$ can be calculated.

There are several reasons for the deviation to an ideal diode. One reason is again related to Fermi level pinning. In this connection surface states start to act as donors or acceptors. Because of this the Fermi level becomes 'pinned' at the surface. Hence a space charge layer is formed, similar to a diodes space charge layer. This decreases the possibility of forming an ideal p-n junction and thus increases the ideality factor to be $n > 1$. Also structural defects in the NWs play an important role, increasing the resistances. Finally one has to consider the junction between the p and n-doped to take place rather continuous than abrupt, also obstructing the ideal diode behavior.

From the four samples shown in Fig. 10, the ideality factor of the NWs of sample (a) (the same InP NWs, but without a passivation layer) has been investigated before[6] with the outcome of the much greater mean value of $4,8 \pm 1,5$ before cleaning the sample, and $4,9 \pm 1,1$ after cleaning. There the spread between ideality factors of the individual NWs was significantly larger, manifested in the great standard deviations. Because the NWs here have been passivated, there are much fewer recombinations at the surface, which cause a lower ideality factor than without the SiO_2 layer.

Important at this point is also a study,[35] which tested the effect of piranha etching on InP NWs. The performance improved after reducing the amount of surface oxides, a great increase of conductance (about one order of magnitude at 1 V) was recorded.

4.2.2 Photovoltaic-response of InP nanowires

Dealing with highly doped InP *p*-*n* junction NWs, one could expect a significant photovoltaic-response. There are several papers[5,6,10,33] with the purpose of measuring the current change of InP NWs, like described in section 2.1.3. Unfortunately there has been no measurable effect within this thesis work. But because a serious amount of work was put into this attempt, it is going to be mentioned briefly.

Because of the comparatively small band gap of InP (1, 34 eV, being equivalent to a wavelength of about 920 nm) all visible light should have enough energy to excite electrons to the conduction band. After trying out a point-shaped red laser with a wavelength of $\lambda = 650\,\text{nm}$ without results, a green laser with $\lambda = 532\,\text{nm}$ was mounted in case the photon energy was decreased in the process. Without achieving any differences in the *I*-*V* behavior another line shaped red laser of $\lambda = 656\,\text{nm}$ was installed. Thus the lack of photoelectric response does not seem to be caused by the intensity, nor the wavelength of the laser.

Furthermore the angle in which the beam hits the surface was investigated. Because the NWs are standing so close to each other, there might be a shadowing effect of the wires so the light only reaches the very top end of the wires. Because the photons do not reach the depleted region of the *p*-*n* junction, they are not able to cause a perceivable current change in the *I*-*V* curve. Working in the high vacuum chamber limited the possible angles very much. The red laser with $\lambda = 656\,\text{nm}$ was mounted in both ways described in section 3.4, directly pointing at the sample, as well as using its light reflection. Nevertheless none of the tested angles resulted in a measurable photoelectric response.

Unlike all previous measurements which caused a current shift, the research here has been performed on NWs coated with a passivation layer. This could contribute to a more difficult absorption of light. This outcome strongly emphasizes the necessity for further research in this area.

Conclusion and outlook

The conductivity of different III-V NWs under structural and external layer changes was investigated and further developed in the previous discussion. In the process of measuring electrical properties of InAs and InP NWs standing upright on the substrate they have been grown on, the technique of STM has been used not only in the conventional way. In a second step the method of top contacting was used to apply a bias, representing a non-destructive, surface sensitive way of recording the NWs' *I*-*V* curve(s). Being able to produce reproducible *I*-*V* measurements, and actually being able to use all of the recorded measurements, but one, when the external voltage source overloaded (compared to a usability of 50% with the method of wiping the wires of the substrate[31]), underlines the effectiveness of this method.

Because only few papers have been published within the field of contacting single NWs, this work is of special importance. These results are a first step towards truly understanding the conductivity properties and what factors they are influenced by. This thesis represents a first study on many aspects which will experience further investigation.[39,40]

As one part of the research the conductance of InAs NWs containing ZB and WZ structures was studied. The resistances of single NWs were found to decrease strongly, by one order of magnitude, after hydrogen cleaning. Additionally one third of the measured curves before cleaning showed a rectifying, non-Ohmic behavior possible due to multiple structural interfaces. After cleaning the sample these strong irregularities disappeared completely (within this limited amount of measurements). The outcome supports the assumption that the transition between WZ and ZB structures limits the conductivity of NWs especially if the NWs are oxidized. Furthermore hydrogen cleaning seems to improve the conductivity and homogeneity of NWs, stressing the large and so far unused potential of InAs NWs for electrical applications.

With quantities of 12 and 8 NWs the amount of measurements were in the originally set target range. Nonetheless, to further validate this statement, more data and research is required. To apply proper statistics especially for differentiating between Ohmic and non-Ohmic behavior, significantly more data is needed. Also one should measure the conductance of NWs with only one structure (ZB or WZ) for comparison.

As a second focus the conductivity of InP NWs was measured. Even though adding a passivation layer in the process of creating solar cells is common practice, there has never been a paper published on single wire conductance with a SiO_2 layer. Hence this research fills the gap and depicts an important step towards a comprehensive understanding of photovoltaic cells and the influence of subsequent processing steps. The obtained ideality factor of $2,4 \pm 0,2$, gained from a quantity of 10 measurements, is much smaller than the factor measured before at a reference sample without the passivation layer. This affirms the necessity to passivate NWs in the process of building solar cells. However the attempt to trigger a photovoltaic response has failed so far. This holds some very interesting questions which need to be answered: Does this sample show a photovoltaic response at all? Is it stronger angle-dependent than its counterpart without passivation layer? And why? One possibility would be to measure the sample in air, which features possibilities for larger angles and higher intensities. Also one could test the same setting with a similar sample which is known to show a response to light. Finally there are still two more samples, see in Fig. 10(b) and (c), to be measured and analyzed to complete the initiated project.

Looking at a bigger scale: This field implies a huge potential and numerous interesting in-depth study possibilities to work towards producing low-cost, highly efficient NW solar cells, which are strongly light absorbent and effective carrier collection while requiring only small amount of material.

References

1. J. a. del Alamo, *Nanometre-scale electronics with III–V compound semiconductors*, Nature **479**, 317–323 (2011).
2. C. M. Lieber, *Semiconductor nanowires: A platform for nanoscience and nanotechnology*, in Inec 2010 - 2010 3rd int. nanoelectron. conf. proc. (2010), pp. 5–6.
3. M. T. Borgström et al., *Precursor evaluation for in situ InP nanowire doping*, Nanotechnology **19**, 445602 (2008).
4. L. Wernersson, C. Thelander, E. Lind, and L. Samuelson, *III-V Nanowires - Extending a Narrowing Road*, Proc. IEEE **98**, 2047–2060 (2010).
5. J. Wallentin et al., *InP nanowire array solar cells achieving 13.8% efficiency by exceeding the ray optics limit.* Science **339**, 1057–60 (2013).
6. J. Colvin, *(Opto) Electrical Characterization of III-V Semiconductor Nanowires Using SPM Techniques*, M.Sc. thesis (Lund University, 2014).
7. P. Hofmann, *Solid state physics* (WILEY-VCH Verlag GmbH & Co. KGaA, Weinheim, 2008).
8. OxfordDictionaries, *Photovoltaic*, (cited: April, 2^{nd} 2015) `http://www.oxforddictionaries.com/us/definition/american_english/photovoltaic`.
9. X. Duan et al., *Indium phosphide nanowires as building blocks for nanoscale electronic and optoelectronic devices.* Nature **409**, 66–69 (2001).
10. H. Goto et al., *Growth of core-shell inP nanowires for photovoltaic application by selective-area metal organic vapor phase epitaxy*, Appl. Phys. Express **2**, 035004 (2009).
11. M. Law et al., *Nanowire dye-sensitized solar cells.* Nat. Mater. **4**, 455–459 (2005).
12. Y. Li, F. Qian, J. Xiang, and C. M. Lieber, *Nanowire electronic and optoelectronic devices*, Mater. Today **9**, 18–27 (2006).
13. R. S. Wagner and W. C. Ellis, *The vapor-liquid-solid mechanism of crystal growth and its application to silicon*, Trans. Metall. Soc. AIME **233**, 1053–1064 (1965).
14. M. Messing, *Gold Particles for Growth of Semiconductor Nanowires*, Licentiate (Lund University, 2009).
15. K. A. Dick, *A review of nanowire growth promoted by alloys and non-alloying elements with emphasis on Au-assisted III-V nanowires*, Prog. Cryst. Growth Charact. Mater. **54**, 138–173 (2008).
16. O. Persson, *Surface studies of III-V nano devices*, licentiate thesis (Lund university, 2013), p. 48.
17. M. T. Borgström et al., *Nanowires with promise for photovoltaics*, IEEE J. Sel. Top. Quantum Electron. **17**, 1050–1061 (2011).
18. S. Lehmann et al., *A general approach for sharp crystal phase switching in InAs, GaAs, InP, and GaP nanowires using only group v flow*, Nano Lett. **13**, 4099–4105 (2013).
19. M. Hjort et al., *Electronic and Structural Di ff erences between Wurtzite and Zinc Blende InAs Nanowire Surfaces : Experiment and Theory*, ACS Nano, 12346–12355 (2014).
20. C. Thelander et al., *The electrical and structural properties of n-type InAs nanowires grown from metal-organic precursors.* Nanotechnology **21**, 205703 (2010).

21. E. P. A. M. Bakkers, M. T. Borgström, and M. a. Verheijen, *E pitaxial Growth of III – V Nanowires on Group IV Substrates*, MRS Bull. **32**, 117–122 (2007).

22. M. A. Green et al., *Solar cell efficiency tables (version 41)*, Prog. Photovoltaics Res. Appl. **21**, 1–11 (2013).

23. S. Today, *Sol voltaics doubles gaas nanowire array solar efficiency record to 15.3%*, (cited: April, 16^{th} 2015) `http://www.semiconductor-today.com/news_items/2015/mar/solvoltaics_180315.shtml`.

24. PV-Tech, *Sol voltaics touts single layer gaas nanowire coated solar cell efficiency record*, (cited: April, 16^{th} 2015) `http://www.pv-tech.org/news/sol_voltaics_touts_single_layer_gaas_nanowire_coated_solar_cell_efficiency`.

25. S. A. A. Abadizadeh, *Rip off and characterization of nanowire ensembles for photovoltaic applications Acknowledgement :* PhD thesis (2013).

26. J. Kupec, R. L. Stoop, and B. Witzigmann, *Light absorption and emission in nanowire array solar cells*, Opt. Express **18**, 27589–27605 (2010).

27. G. Binnig, H. Rohrer, C. Gerber, and E. Weibel, *Surface studies by scanning tunneling microscopy*, Phys. Rev. Lett. **49**, 57–61 (1982).

28. R. B. Ernst Meyer, Hans Josef Hug, *Scanning probe microscopy* (Springer, Heidelberg, 2004).

29. J. Tersoff and D. R. Hamann, *Theory of the scanning tunneling microscope*, Phys. Rev. B **31**, 805–813 (1985).

30. M. Scheffler et al., *Diameter-dependent conductance of InAs nanowires*, J. Appl. Phys. **106**, 2009–2012 (2009).

31. D. B. Suyatin et al., *Sulfur passivation for ohmic contact formation to InAs nanowires*, Nanotechnology **18**, 105307 (2010).

32. R. Timm et al., *Current - Voltage Characterization of Individual As-Grown Nanowires Using a Scanning Tunneling Microscope*, Nano Lett. **13**, 5182–5189 (2013).

33. S. M. Sedlak, *Scanning Probe Microscopy on Semiconductor Nanowires for Photovoltaics*, B.Sc. thesis (Lund University, 2013).

34. D. W. Moon et al., *Low sputter damage of metal single crystalline surfaces investigated with medium energy ion scattering spectroscopy*, Appl. Surf. Sci. **150**, 235–243 (1999).

35. Y. Cui et al., *Efficiency enhancement of InP nanowire solar cells by surface cleaning.* Nano Lett. **13**, 4113–7 (2013).

36. S. Nannarone and M. Pedio, *Hydrogen chemisorption on III-V semiconductor surfaces*, 2003.

37. C. Thelander et al., *Effects of crystal phase mixing on the electrical properties of InAs nanowires*, Nano Lett. **11**, 2424–2429 (2011).

38. M. H. M. Van Weert et al., *Large redshift in photoluminescence of p -doped InP nanowires induced by Fermi-level pinning*, Appl. Phys. Lett. **88**, 1–3 (2006).

39. O. Persson et al., *Change of band alignment between wurtzite and zinc-blende segments in inas nanowires upon surface oxidation*, to be published.

40. J. Colvin et al., *Photovoltaic properties of individual inp nanowires during processing steps and surface modification*, to be published.